Acta Pharmacologica Sinica

www.nature.com/aps

ARTICLE

QAP14 suppresses breast cancer stemness and metastasis via activation of dopamine D1 receptor

Ling Yong[1], Ye Yao[1], Guo-shu Chen[2], Xiao-xue Yan[2], Yu-chen Guo[1], Meng-yi Han[1], Jun-sheng Xue[1], Wei-zhe Jian[1] and Tian-yan Zhou[1]

Breast cancer is the second leading cause of cancer-related mortality in women, mainly due to metastasis, which is strongly associated with cancer stemness. Our previous studies showed that the eradication of cancer stem-like cells (CSCs) may be related to the activation of dopamine D1 receptor (D1DR). This study aimed to explicitly demonstrate the target-role of D1DR activation in antimetastatic therapy and to investigate the potential efficacy and the underlying D1DR-related mechanisms of QAP14, a new oral compound. 4T1, MDA-MB-231, and D1DR-knockout 4T1 (4T1-D1DR) cells were selected for in vitro study, while 4T1 and 4T1-D1DR cells were further used to establish a mouse allograft model for in vivo study. Our results showed that D1DR is abundantly expressed in both 4T1 and MDA-MB-231 cells and that knocking out D1DR in 4T1 cells accelerated migration and invasion in vitro as well as lung metastasis in vivo. QAP14 inhibited colony formation, cell motility, mammosphere formation and CSC frequency, induced CSC apoptosis and D1DR expression, and increased cAMP/cGMP levels. Additionally, QAP14 showed inhibitory effects on tumor growth and lung metastasis with acceptable safety in vivo. Knocking out D1DR almost completely abolished the efficacy, confirming that QAP14 exhibits its anti-CSC and antimetastatic effects through D1DR activation. The underlying mechanisms involved suppression of the nuclear factor κB (NF-κB)/protein kinase B (Akt) pathway and consequent downregulation of both epithelial-to-mesenchymal transition (EMT) process and cancer stemness. In summary, our findings suggest a potential candidate compound, QAP14, as well as a potential target, D1DR, for metastatic breast cancer therapy.

Keywords: metastatic breast cancer; dopamine D1 receptor; cancer stemness; lung metastasis; cell motility; QAP14

Acta Pharmacologica Sinica (2022) 43:1001–1012; https://doi.org/10.1038/s41401-021-00701-9

INTRODUCTION

In women, breast cancer is the second leading cause of cancer-related mortality, which results primarily from metastasis [1]. Furthermore, metastasis is responsible for up to 90% of all cancer-associated deaths. However, therapies for metastatic breast cancer are rather limited [2]; hence, it is highly desirable to develop new treatment strategies.

Cancer stem-like cells (CSCs), which are closely associated with poor clinical outcomes, represent a specific population of cells with the ability to self-renew and generate a new tumor [3]. Breast cancer is regarded as a stem cell disease characterized by the existence of CSCs that proliferate and differentiate to produce advanced metastatic disease, which may partially explain why traditional chemotherapies targeting differentiated tumor cells fail to eradicate CSCs and cure metastatic cancers. In recent years, CSC-specific drugs such as salinomycin [4], metformin [5], vitamin D3 [6], and piperine [7] have been in development and have received considerable attention. However, the similarities in features and signaling pathways between CSCs and human pluripotent stem cells (hPSCs) may lead to indiscriminate killing of cells.

Drugs targeting dopamine receptors (DRs) are capable of acting specifically on CSCs while sparing normal hPSCs due to the specific expression of DRs on CSCs [8]. DRs are classified as D1-class receptors (D1DR and D5DR) and D2-class receptors (D2DR, D3DR, and D4DR). Several antipsychotic D2DR antagonists, including thioridazine [8], sulpiride [9] and trifluoperazine [10], have been demonstrated to be effective for the inhibition of CSCs. Our previous study found that dopamine (DA) can decrease the CSC frequency in drug-resistant breast cancer and non-small cell lung cancer by D1DR activation [11, 12]. The D1DR agonists fenoldopam (FEN) and l-stepholidine (l-SPD) also exhibited anti-CSC effects and further reduced lung metastasis in a 4T1 allograft model [13]. However, these studies did not directly demonstrate that D1DR is the target of these drugs' actions.

In addition, antipsychotic drugs can cross the blood–brain barrier, which may cause unexpected effects on the central nervous system. DA, FEN, and l-SPD can only be administered intravenously, and their plasma elimination half-lives are extremely short (usually a few minutes). These disadvantages may limit their clinical application for cancer treatment. Therefore, the N-arylpiperazine-containing compound C2 was originally synthesized and was shown to have high affinity for D1DR and anti-CSC effects on pancreatic cancer [14]. In addition, the compound C17, an analog of C2, was shown to visibly decrease the CSC population in metastatic breast cancer [15]. The underlying mechanisms were only preliminarily investigated, and the D1DR antagonist SCH 23390 (abbreviated SCH) was used instead of genetic engineering

[1]Beijing Key Laboratory of Molecular Pharmaceutics and New Drug Delivery System, Department of Pharmaceutics, School of Pharmaceutical Sciences, Peking University, Beijing 100191, China and [2]Chemical Basic Laboratory, School of Chemistry and Chemical Engineering, Guangzhou University, Guangzhou 510006, China
Correspondence: Tian-yan Zhou (tianyanzhou@bjmu.edu.cn)

Received: 8 January 2021 Accepted: 17 May 2021
Published online: 28 June 2021

techniques such as knockout of D1DR to verify the potential target. Additionally, the underlying mechanisms associated with activation of D1DR in addition to the epithelial-to-mesenchymal transition (EMT) process remain to be explored. Therefore, it is of great value to explicitly demonstrate the relationship between D1DR activation and antimetastatic efficacy as well as to comprehensively investigate D1DR-related mechanisms.

The aim of this study was to explore the inhibitory effect of a new aminoquinazoline aryl piperazine derivative, QAP14, on breast cancer metastasis as well as to comprehensively investigate the underlying mechanisms and to directly confirm the role of D1DR activation in antimetastatic therapy. This study may identify a potential candidate for the treatment of metastatic breast cancer.

MATERIALS AND METHODS

Reagents and antibodies

QAP14 (purity >95%, structure shown in Fig. 1a) was synthesized by Professor Guo-shu Chen's laboratory, Guangzhou University, China. Hoechst 33342 (14533-100MG) and SCH 23390 (D054-10MG) were obtained from Sigma-Aldrich, USA. Sunitinib (SUN) was purchased from Meilun Biotech Co., Ltd., China. The anti-D1DR antibodies used for immunofluorescence staining (ab20066) and for Western blotting (sc-33660) were purchased from Abcam, USA, and Santa Cruz Biotechnology Inc., USA, respectively. Anti-rabbit IgG (HRP-linked) (7074), anti-mouse IgG (HRP-linked) (7076), anti-NF-κB p65 (8242), anti-phospho-NF-κB p65 (3033), anti-IκBα (4814), anti-phospho-IκBα (2859), anti-IKKβ (8943), anti-phospho-IKKα/β (2697), anti-Akt (4691), anti-phospho-Akt (4060), anti-E-cadherin (3195), anti-N-cadherin (13116), anti-Vimentin (5741), anti-Slug (9585), anti-Snail (3879), anti-ZO-1 (8193) and anti-Histone H3 (4499) antibodies were obtained from Cell Signaling Technology, USA. Anti-rabbit IgG H&L (FITC) (ab6717), anti-MMP2 (ab37150) and anti-β-actin (ab179467) antibodies were purchased from Abcam.

Cell lines and cell culture

The mouse mammary carcinoma cell line 4T1 and human breast cancer cell line MDA-MB-231 were purchased from the Institute of Materia Medica, Academy of Medical Sciences, China. The D1DR-knockout 4T1 (4T1-D1DR) cell line was constructed using CRISPR/Cas9 and verified by Cyagen Biosciences Inc., China. The gRNA sequences used for establishment of the 4T1-D1DR cell line are as follows:

gRNA1: 5'-TAACCTCTGTGTGATCAGCGTGG-3'
gRNA2: 5'-CCAGCCCTTTCCAGTATGAGAGG-3'
gRNA3: 5'-AAGTCCATGCTACGCTAATCAGG-3'

4T1 and 4T1-D1DR cells were cultured in RPMI-1640 medium, while MDA-MB-231 cells were cultured in Leibovitz's L-15 medium. Both media were supplemented with 10% fetal bovine serum (FBS) (PAN-Biotech, Germany) and 1% penicillin-streptomycin (GIBCO, USA). Cells were maintained in a humidified atmosphere with 5% CO_2 at 37 °C and subcultured when ~80% confluent.

Colony formation assay

4T1, 4T1-D1DR, and MDA-MB-231 cells (1500 cells/well) were seeded in six-well plates. After 24 h of incubation, the cells were treated with 2 or 8 μM QAP14 for 48 h, with or without 2 μM SCH, a D1DR antagonist [15]. Then, the culture medium was replaced with drug-free medium, and the cells were incubated until the colonies contained ~50 cells on average. The colonies were subsequently fixed with methanol, stained with crystal violet solution and counted using an ImageQuant TL 7.0 (GE Healthcare, USA).

Sphere formation assay

4T1 and MDA-MB-231 cells (2×10^4 cells/well) were plated in ultra-low attachment six-well plates in spheroid medium (DMEM-Ham's F12 medium containing 10% B27, 10 ng/mL basic fibroblast growth factor (bFGF), 20 ng/mL epidermal growth factor and 5 μg/mL insulin). Cells were incubated for 5 days and were then treated with 8 μM QAP14 and 2 μM SCH alone or in combination for 2 days. Then, spheroids were photographed using an IX70 inverted fluorescence microscope.

Detection of CSC frequency

After 5 days of incubation and 2 days of treatment with 8 μM QAP14 alone or in combination with 2 μM SCH, mammospheres formed from 4T1 cells (4T1-BCSCs) and MDA-MB-231 cells (MDA-MB-231-BCSCs) were collected, dissociated, and suspended. Aldehyde dehydrogenase (ALDH), a stem cell marker, was detected with an ALDEFLUOR™ Kit (STEMCELL Technologies, Canada). For each sample, a test group and a negative control group treated with diethylaminobenzaldehyde, an ALDH inhibitor, were established. After incubation for 45 min at 37 °C, the CSC frequency was determined with a FACSCalibur flow cytometer (Becton Dickinson, USA).

Detection of apoptotic cells

The proportion of apoptotic cells was evaluated using a FITC Annexin V Apoptosis Detection Kit with PI (BioLegend, USA). After treatment with 4 or 8 μM QAP14 and/or 2 μM SCH for 48 h, 4T1 and MDA-MB-231 spheres were dissociated, washed and resuspended in 400 μL of cold Annexin-V labeling buffer. Next, the cells were stained with 10 μL of FITC-labeled Annexin-V antibody for 10 min and subsequently incubated with 5 μL of PI on ice for another 5 min in the dark. The apoptotic cell frequency was determined with a FACSCalibur flow cytometer (Becton Dickinson).

Wound healing assay

4T1, 4T1-D1DR, and MDA-MB-231 cells were seeded in six-well plates at densities of 2×10^4 cells/well, 2×10^4 cells/well and 1.5×10^4 cells/well, respectively; incubated overnight for attachment; and treated with 2, 4, or 8 μM QAP14 in the presence or absence of 2 μM SCH. Scratch wounds were created with sterile 200 μL pipette tips and rinsed with PBS. After 12 h of treatment, the cells were fixed with methanol, and the wounded area was photographed under a BDS 400 inverted microscope (Chongqing Optec Instrument, China) to measure the migration distance.

Transwell migration and invasion assays

For the transwell migration assay, cells suspended in serum-free medium were seeded in the upper chambers of 24-well plates at a density of 3×10^4 cells per well, and 500 μL of medium supplemented with 10% FBS was added to the lower chambers. Vehicle, QAP14 (2, 4, or 8 μM) and SCH (2 μM) were added to the medium in both the upper and lower chambers. After 16 h, the upper surface of the filter was wiped to remove all attached cells, and the migrated cells were fixed with methanol and stained with 0.5% crystal violet solution. Images were acquired using an IX70 inverted fluorescence microscope, and the migrated cells were counted.

For the transwell invasion assay, the upper chamber membrane was coated with a 10% matrix gel, and the lower chamber contained 600 μL of medium containing 20% FBS. Cells that invaded through the membrane into the lower chamber were imaged and quantitated after treatment for 32 h (4T1 and 4T1-D1DR cells) or 24 h (MDA-MB-231 cells). The procedures for the remaining steps were similar to those used for the transwell migration assay.

Immunofluorescence staining

For detection of D1DR expression, 4T1, 4T1-D1DR and MDA-MB-231 cells were seeded in 15 mm glass-bottom confocal dishes and cultured for 24 h. To assess the effect of different compounds, 4T1 cells were cultured for 12 h and incubated with 4 or 12 μM QAP14, 2 μM SCH or a combination of 4 μM QAP14 and 2 μM SCH for another 12 h. After being washed with PBS, cells were fixed with 4% paraformaldehyde for 20 min; blocked with 10% BSA solution containing 0.1% Tween 20, 0.3% Triton X-100 and 22.52 mg/mL glycine for 1 h; and incubated with primary antibodies against D1DR (1:1000), NF-κB p65 (1:500) or phospho-NF-κB p65 (1:200) overnight at 4 °C. Then, cells were incubated in the dark with a FITC-conjugated secondary antibody (1:1000) for 1 h. Hoechst 33342 (Hoechst; 5 μg/mL) was used to stain nuclei for 30 min before visualization under a TCS SP8 confocal microscope (Leica, Germany).

Western blotting analysis

Total cellular protein was obtained by lysing cells with RIPA lysis buffer containing 1% PMSF (and 1% proteinase inhibitor for phosphorylated protein detection), while nuclear protein was extracted using a Nuclear and Cytoplasmic Protein Extraction Kit (Beyotime, China). The protein concentration was determined with a Protein BCA Assay Kit (Beyotime, China). Proteins (30–50 μg) were separated by 10% SDS-PAGE and transferred to polyvinylidene difluoride membranes. The membranes were then blocked with 5% BSA for 1.5 h and incubated at 4 °C overnight with primary antibodies, which were later detected with secondary antibodies (HRP-anti-rabbit (1:6000) or HRP-anti-mouse (1:1000) IgG) at room temperature for 1.5 h. Finally, the target proteins were quantified with an Amersham Imager 600 (GE Healthcare, USA) after visualization with ECL solution.

Measurement of cyclic adenosine monophosphate (cAMP) and cyclic guanosine monophosphate (cGMP)

4T1 cells were treated with 8 μM QAP14 for 15 min before being collected for testing. cAMP and cGMP concentrations were measured using a Cyclic AMP Select ELISA Kit (Cayman, USA) and a Cyclic GMP ELISA Kit (Cayman), respectively.

Animals

Five-week-old female BALB/c mice weighing 16–18 g were purchased from Beijing Vital River, China, and were housed under multibarrier and specific-pathogen-free conditions with a temperature of 22–26°C and a relative humidity of 50%–60% on a 12 h light/12 h dark cycle. All experimental procedures were conducted following the guidelines of the Institutional Animal Care and Use Committee of Peking University.

In vivo lung metastasis models

For the 4T1 and 4T1-D1DR allograft models, 1×10^6 4T1 or 4T1-D1DR cells in FBS-free medium were injected into the fourth breast fat pad of mice to establish the metastatic breast cancer model.

Experiment 1 (Exp1): In the 4T1 allograft model, to investigate the efficacy of different regimens on lung metastasis, mice were randomly divided into seven groups ($n = 6$) when the average tumor volume was ~80 mm^3. The dosing regimens were as follows: vehicle control; QAP14 20 mg/kg, QAP14 40 mg/kg and SUN 10 mg/kg dissolved in 1,2-propanediol solution and administered orally daily; SCH 0.05 mg/kg dissolved in 0.9% saline solution and administered intratumorally daily; and a combination of QAP14 40 mg/kg and SCH as well as a combination of QAP14 40 mg/kg and SUN coadministered daily. The tumor volume was calculated with the formula $0.5 \times \text{length} \times \text{width}^2$. Mice were sacrificed on the 21st day after inoculation, and tumors as well as major organs were harvested and weighed. Lungs were stained with Bouin's fixative, and metastases with diameters greater than or equal to 0.3 mm were counted. Later, lungs were embedded in paraffin, sliced into sections, stained with hematoxylin-eosin (H&E) and photographed with a Vectra Polaris Automated Quantitative Pathology Imaging System (PerkinElmer, USA).

Exp2: To explore the effect of QAP14 on the overall survival of 4T1 tumor-bearing mice, when the average tumor volume was 80 mm^3, mice were randomly assigned to the control group or the treatment group ($n = 5$). QAP14 was administered orally (20 mg/kg every day) to mice in the treatment group, while vehicle solvents were given as controls. The survival time of each mouse was recorded.

Exp3: To clarify the relationship between QAP14's antimetastatic efficacy and D1DR activation, mice were randomly divided into three groups ($n = 5$): mice in one group were inoculated with 4T1 cells, and mice in the other groups were inoculated with 4T1-D1DR cells. When the average tumor volume was ~80 mm^3, the 4T1-D1DR allograft-bearing mice were treated with vehicle solvents or 20 mg/kg QAP14. In parallel, 4T1 tumor-bearing mice were administered vehicle solvents. Mice were sacrificed, and lungs were harvested on the 21st day after inoculation.

For the 4T1-BCSC allograft model, 1×10^5 4T1 mammosphere cells in FBS-free medium were injected into the fourth breast fat pad of mice. After 2 days, the mice were randomly divided into three groups ($n = 5$), and vehicle, QAP14 20 mg/kg or 40 mg/kg was then administered intragastrically every day. On the 17th day after inoculation, the mice were sacrificed, and tumors and lungs were collected.

Safety evaluation of QAP14

The safety profile of QAP14 was assessed in Exp1 by monitoring body weight, examining blood samples, calculating organ indexes and conducting H&E staining. Body weight was recorded throughout. Blood samples were collected from the postorbital venous plexus of mice and quickly evaluated with a Hemavet 950 hematology system (Drew Scientific, USA). Major organs were collected, weighed, fixed with 10% formalin solution, and stained with H&E for histopathological observation using a Vectra Polaris Automated Quantitative Pathology Imaging System (PerkinElmer, USA). Organ indexes were calculated according to the following equation: organ index (%) = organ weight/(body weight − tumor weight) × 100%.

Statistical analysis

The results are presented as the mean ± SD values, and statistical analysis was performed with Microsoft Excel 2016 (Microsoft Corporation, USA) and GraphPad Prism 8.0 (GraphPad Software Inc., USA). Student's *t*-test and one-way ANOVA followed by the Bonferroni post hoc test were used for intergroup comparisons. A value of $P < 0.05$ was considered statistically significant.

RESULTS

QAP14 suppresses the stemness and tumorigenic ability of metastatic breast cancer

Clonogenicity is an important feature and a sensitive indicator of CSCs that ensures their proliferation and differentiation patterns, which can be evaluated by colony formation assays [16]. As shown in Fig. 1b, 2 and 8 μM QAP14 reduced the percentage of surviving 4T1 cell colonies from 100% to 86.64% and 48.41% and that of MDA-MB-231 cells from 100% to 81.92% and 29.19%, respectively, indicating that QAP14 significantly suppresses the stemness of breast cancer cells.

The sphere formation assay, which has been widely used for the enrichment of CSCs, evaluates the stemness of a certain cell line [17]. As illustrated in Fig. 1c, 4T1 cells formed round spheres, while MDA-MB-231 cells formed looser and less rounded spheres. Moreover, QAP14 was revealed to inhibit the stem-like population from forming mammospheres in both cell lines.

The capability of QAP14 to reduce the CSC frequency was examined by an ALDEFLUOR assay, which is used to determine the

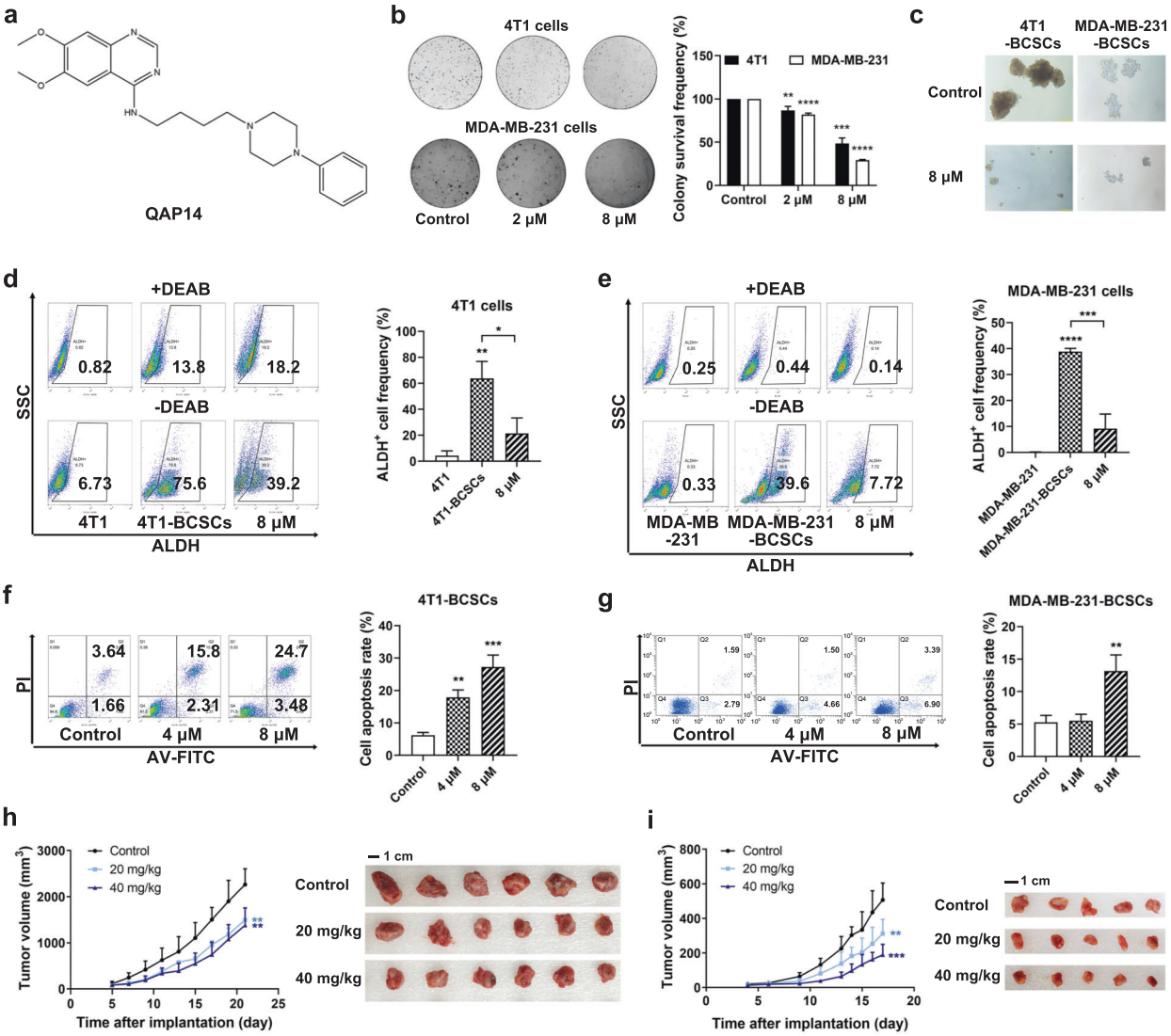

Fig. 1 QAP14 suppressed stemness and tumor growth of metastatic breast cancer. a The molecular structure of QAP14. **b** The effects of QAP14 on the colony formation were investigated in 4T1 and MDA-MB-231 cells after treatment with 0, 2, 8 μM QAP14 for 48 h. Colony survival frequency is expressed relative to the corresponding untreated group ($n = 3$). **c** Mammospheres derived from 4T1 and MDA-MB-231 cells were cultured with 0, 8 μM QAP14 for 48 h and then photographed. The ALDH-positive cell frequency of 4T1-BCSCs (**d**) or MDA-MB-231-BCSCs (**e**) as well as the corresponding adherent cells was detected ($n = 3$). The apoptotic cell proportion of 4T1 (**f**) and MDA-MB-231 (**g**) spheres was determined ($n = 3$). The mammospheres for test of CSC frequency and apoptosis were treated with 0, (4), 8 μM QAP14 for 48 h. In vivo anti-cancer efficacy on 4T1 cell line-derived (**h**) ($n = 6$ per group) or 4T1-BCSCs-derived (**i**) ($n = 5$ per group) allograft models. Tumor volumes were measured every 2–3 days and the tumors were harvested at the end of experiments. The black scale bar indicates 1 cm. Data are presented as mean ± SD. $^{**}P < 0.01$, $^{***}P < 0.001$, $^{****}P < 0.0001$ compared with the corresponding control group (if not indicated).

proportion of cells positive for ALDH, a hallmark of CSCs, in 4T1 and MDA-MB-231 cells. As Fig. 1d shows, the percentage of ALDH-positive cells among 4T1-BCSCs was elevated from 4.23% to 63.75% compared with that in adherent cells, indicating that CSCs were enriched in the mammospheres. After 8 μM QAP14 treatment for 48 h, the percentage of ALDH-positive cells was significantly decreased to 21.49%. A similar increase in the ALDH-positive cell percentage and a comparable inhibitory effect of QAP14 were observed in MDA-MB-231-BCSCs (Fig. 1e). The effect of QAP14 on CSC apoptosis was verified by flow cytometry. As shown in Fig. 1f, g, after treatment with QAP14 for 48 h, both BCSC lines exhibited a dose-dependent increase in apoptotic cells compared with the control groups. These results suggest that the inhibition of cell stemness by QAP14 is associated with a decrease in the CSC frequency and an increase in CSC apoptosis.

To further confirm the effect of QAP14 on CSCs in vivo, 4T1 and 4T1-BCSC allograft models were established for evaluation. Considering that CSCs tend to transfer their properties to normal cancer cells [3], beginning on the 2nd day after inoculation, mice were treated with vehicle solvents or QAP14 (20 or 40 mg/kg). Fig. 1h, i show the antitumor effects of QAP14 on 4T1 and 4T1-BCSC allografts, respectively. The tumors in the control group grew more rapidly in the 4T1 allograft model than in the 4T1-BCSC model. For mice bearing 4T1-BCSC allografts, 4 days after inoculation, subcutaneous tumors were clearly visible at the inoculation site in most mice. The rate at which 4T1-BCSCs formed tumors in the control and low-dose groups was 100% but was only 40% in the high-dose group and eventually increased to 100% on the 9th day, suggesting that QAP14 delayed tumorigenesis. The inhibition rates in the two treatment groups in the 4T1 allograft

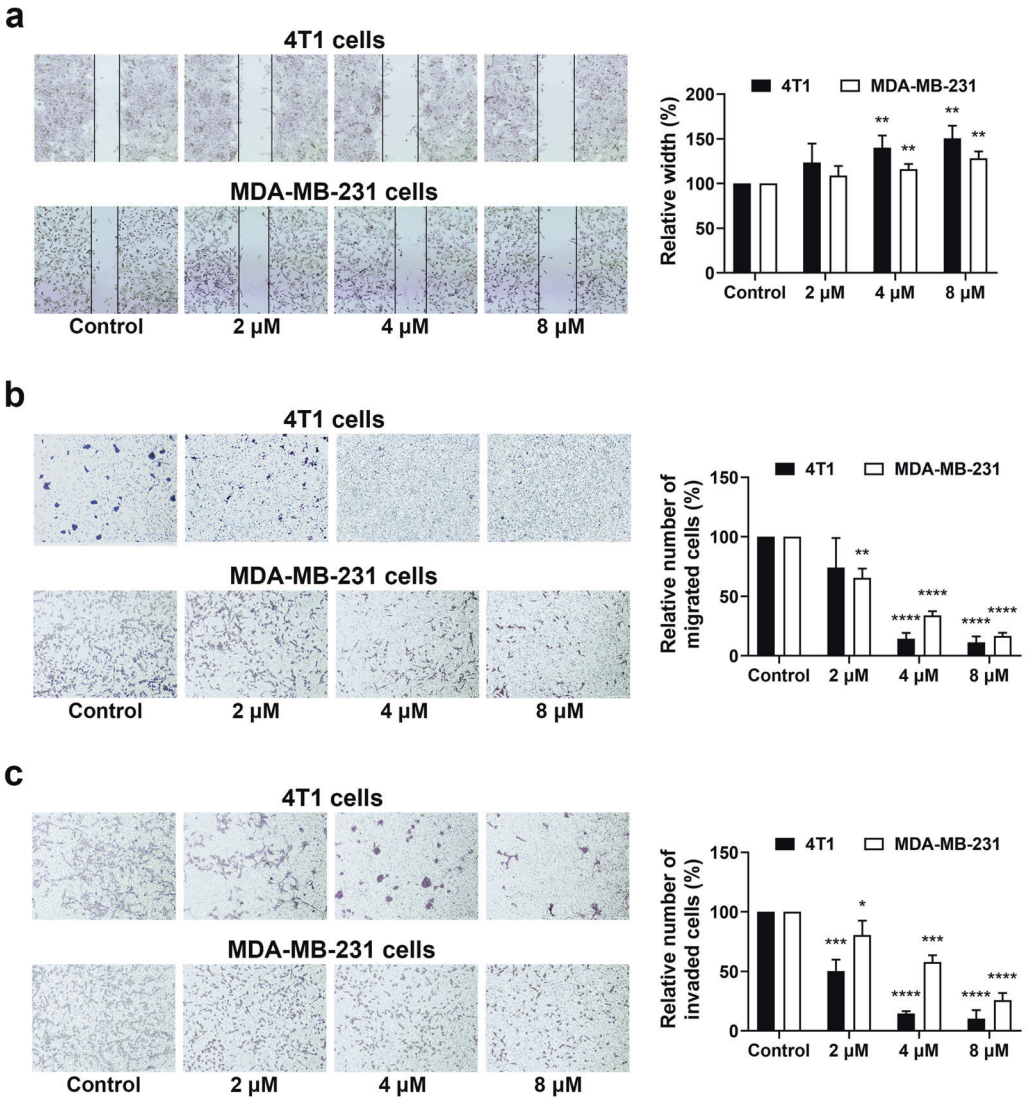

Fig. 2 QAP14 inhibited the motility of metastatic breast cancer cells. a Identical scratches were made on 4T1 and MDA-MB-231 cells. After treatment with 0, 2, 4, 8 μM QAP14 for 12 h, wound widths were measured. **b** Cells were exposed to graded concentrations of QAP14 for 16 h. **c** Cells were cultured with different concentrations of QAP14 for 32 h (4T1 cells) and 24 h (MDA-MB-231 cells). Representative images and quantification of the inhibitory activity on cell migration and invasion were shown. The wound width as well as the number of migrated and invasive cells in the control group was defined as 100%. Data are presented as mean ± SD ($n = 3$ per group). $^{*}P < 0.05$, $^{**}P < 0.01$, $^{***}P < 0.001$, $^{****}P < 0.0001$ compared with the corresponding control group.

model were 33.91% and 39.07% compared to the control group, and those in the 4T1-BCSC allograft model were 38.42% and 62.57%, indicating the enhanced inhibitory effect of QAP14 on 4T1-BCSC allografts. These results revealed that QAP14 inhibited tumor formation and growth partially by decreasing cell stemness.

QAP14 inhibited the motility of metastatic breast cancer cells

To investigate the effect of QAP14 on migratory properties, wound healing and transwell migration assays were used to assess the migration of 4T1 and MDA-MB-231 cells treated with QAP14. Cells treated with QAP14 exhibited significantly less wound closure ability than control cells (Fig. 2a). Similarly, after treatment with QAP14, the number of migrated cells exhibited a dose-dependent decline (Fig. 2b). To demonstrate the function of QAP14 in cell invasion, a transwell invasion assay was conducted. With QAP14 treatment, the number of invading cells was dose-dependently decreased relative to that in the control group (Fig. 2c). These consistent results suggested that QAP14 considerably decreased the motility of metastatic breast cancer cells in vitro.

QAP14 reduced lung metastasis of breast cancer with acceptable safety

Female BALB/c mice bearing 4T1 allografts, a frequently used animal model of lung metastasis, were used to evaluate the antimetastatic activity of QAP14 in vivo. On the 21st day after inoculation, the number and size of lung metastases in the QAP14-treated groups were apparently decreased, and stronger inhibitory efficacy was observed in the 40 mg/kg group than in the 20 mg/kg group (Fig. 3a). The differences in lung tissue slices stained with H&E between different groups also suggested this finding (Fig. 3b). The peripheral pulmonary tissue of tumor-bearing mice in the control group was severely damaged compared with that of healthy mice, and dense tumor tissue (indicated by the black arrows) was observed. However, after treatment with QAP14, the area of tumor tissue greatly decreased, and the morphology of lung tissue became normal, especially in the high-dose group. Importantly, an increase in overall survival was observed in the QAP14 (20 mg/kg) treatment group, which may have partially resulted from the inhibition of cancer metastasis (Fig. 3c).

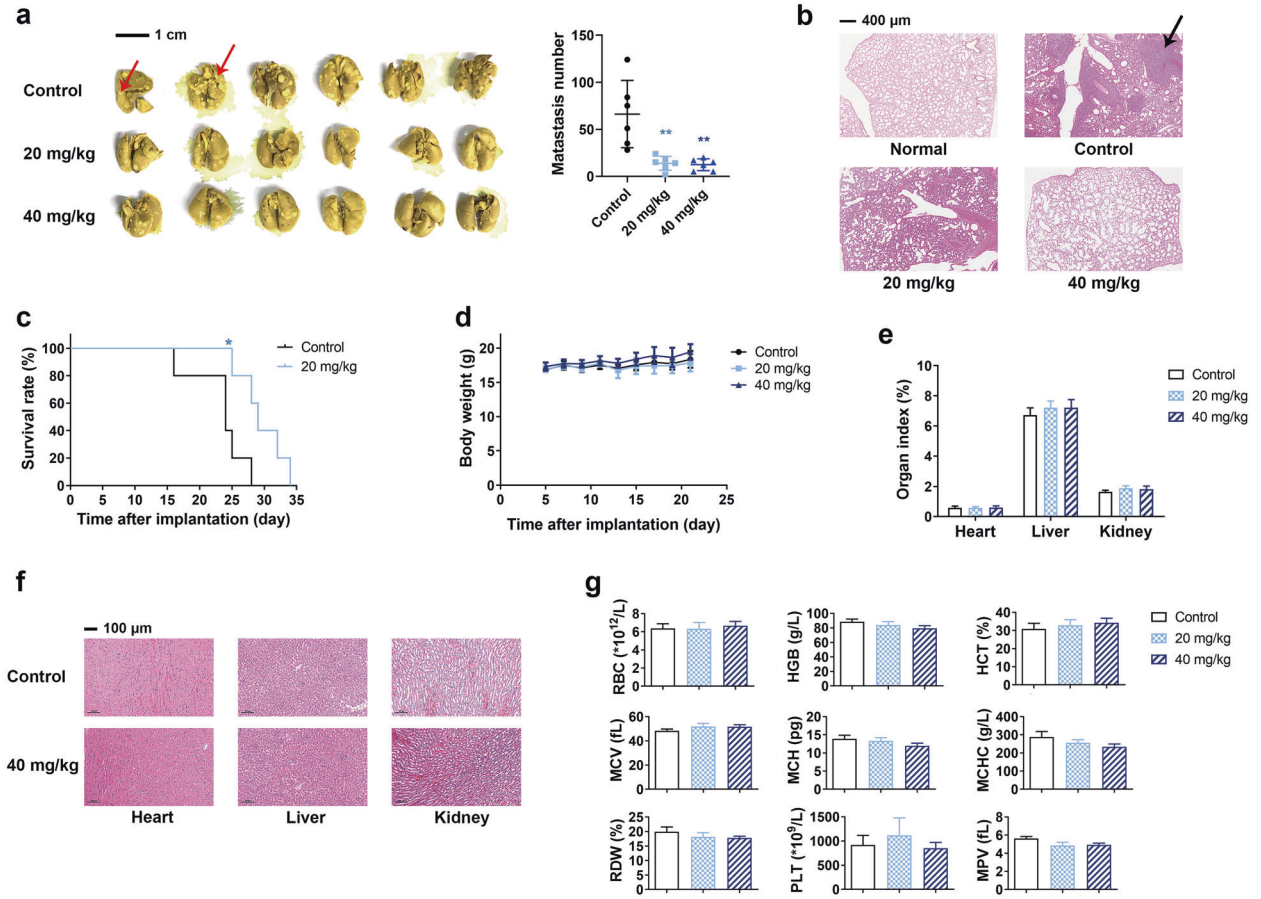

Fig. 3 The anti-metastasis effect and preliminary safety evaluation of QAP14 in 4T1 allograft model. **a** Mice bearing 4T1 tumors were treated with vehicle control, QAP14 20 mg/kg, or QAP14 40 mg/kg daily. On the 21st day after inoculation, the lungs were removed and photographed ($n = 6$). The number of metastases with diameter greater than or equal to 0.3 mm was counted. The black scale bar indicates 1 cm and the red arrow indicates the metastases. **b** The histological sections of lungs were shown and the black arrow indicates the metastatic tissue. The black scale bar indicates 400 μm. **c** An increase in the life span was observed in the QAP14 20 mg/kg group compared with the control group ($n = 5$). **d** Body weights of the mice in each group were monitored throughout the experiment ($n = 6$). **e** Hearts, livers as well as kidneys were taken out and weighed and the organ indexes were calculated ($n = 6$). **f** Representative histopathological images of the major organs in the control and the QAP14 40 mg/kg groups were shown. The black scale bar indicates 100 μm. **g** Hemogram analysis of blood samples in each group ($n = 3$ per group) was conducted before the mice were sacrificed ($n = 6$). RBC red blood cell, HGB hemoglobin, HCT hematocrit, MCV mean corpuscular volume, MCH mean corpuscular hemoglobin, MCHC mean corpuscular hemoglobin concentration, RDW red cell distribution width, PLT platelet count, MPV mean platelet volume. Data are presented as mean ± SD. *$P < 0.05$, **$P < 0.01$ compared with the corresponding control group.

There was no notable reduction in mouse weights in the QAP14 treatment group, indicating little systemic toxicity (Fig. 3d). Moreover, no obvious alterations in organ indexes or morphology were observed in any treatment group (Fig. 3e, f). Hemogram analysis revealed no evidence of blood toxicity after treatment with QAP14 at 20 and 40 mg/kg (Fig. 3g). Together, these results preliminarily showed the safety of QAP14.

QAP14 activated D1DR in metastatic breast cancer cells

The expression of D1DR, which was assumed to be the target of QAP14, was evaluated by immunofluorescence confocal microscopy. As shown in Fig. 4a, b, D1DR (represented by green fluorescence) was expressed in both 4T1 and MDA-MB-231 cells, and QAP14 substantially elevated the expression of D1DR in 4T1 cells. In addition, 4T1 cells treated with 2 μM SCH for 12 h exhibited an obvious decrease in green fluorescence intensity compared with control cells. Moreover, combination treatment with SCH (2 μM) and QAP14 (4 μM) reversed the induction of D1DR expression mediated by treatment with QAP14 alone. The second messengers cAMP and cGMP, whose production can be stimulated when D1DR is activated [18, 19], were evaluated to investigate the effect of QAP14 on D1DR. As shown in Fig. 4c, d, both cAMP and cGMP accumulated significantly in the QAP14-treated group compared to the control group. In addition, the expression of D1DR in 4T1-BCSCs and MDA-MB-231-BCSCs was elevated after the formation of mammospheres (Fig. 4e).

SCH partially antagonized the effects of QAP14 on breast cancer

Given the preliminarily proven inhibitory effects of QAP14 on CSCs, cell motility and lung metastasis, as well as the activation of D1DR, we hypothesized that QAP14 exerts regulatory effects on breast cancer via D1DR activation. To verify this hypothesis, SCH was introduced in pharmacodynamic studies both in vitro and in vivo. SCH monotherapy had a minimal influence on colony growth, sphere formation, and the ALDH-positive cell frequency (Fig. 5a–c). However, the efficacy of QAP14 in suppressing CSC-associated properties was partially or completely antagonized when QAP14 was combined with SCH. Regarding the ability to migrate and invade, the suppressive effects of QAP14 were significantly reversed in the presence of SCH (Fig. 5d–f). Furthermore, the inhibitory effect of QAP14 on lung metastasis in the 4T1 allograft model was offset after treatment with SCH, while SCH

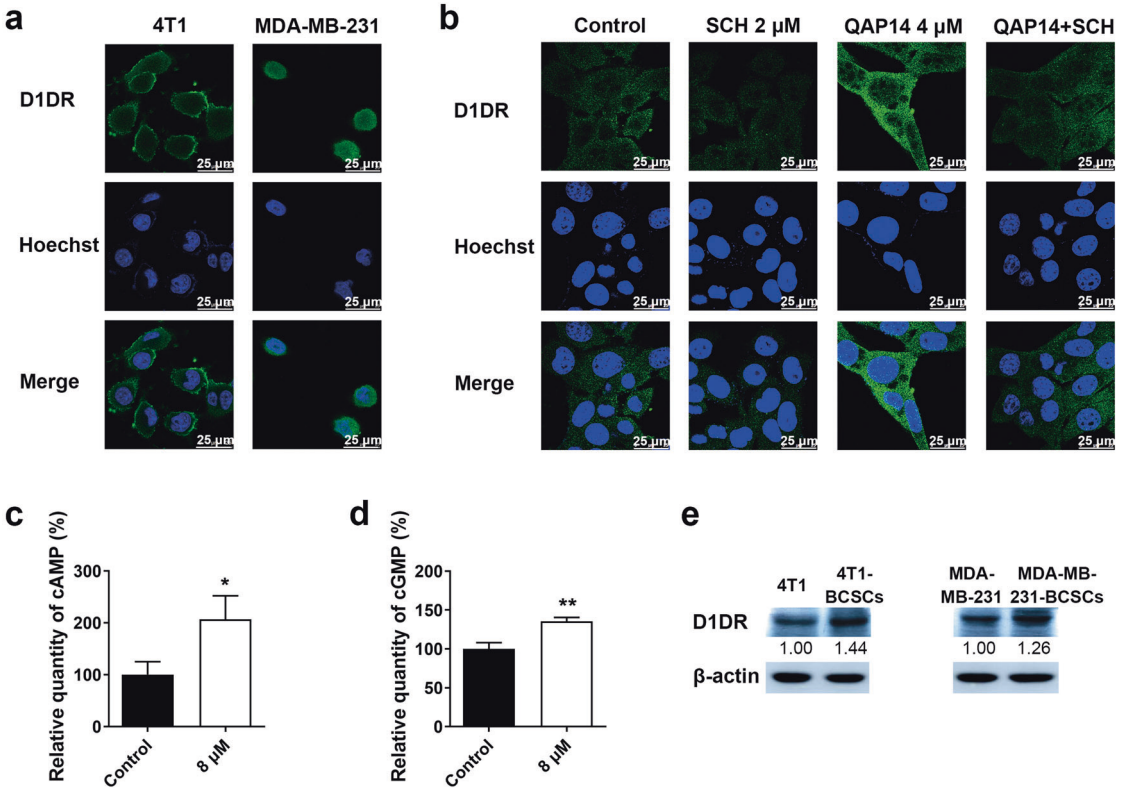

Fig. 4 QAP14 activated D1DR in 4T1 cells. **a**, **b** The expression of D1DR and the effect of QAP14 on D1DR expression were verified through immunofluorescence imaging ($n = 3$). Green fluorescence indicates D1DR expression, while blue fluorescence represents the nuclei. The white scale bar indicates 25 μm. The cAMP (**c**) and cGMP (**d**) quantities of the control and the QAP14 treatment group were detected after treatment for 15 min ($n = 3$). **e** The expression of D1DR in 4T1 and MDA-MB-231 cells as well as the mammospheres formed from the two cell lines was measured by Western blotting. The D1DR quantity in the adherent cells was normalized as "1" to see the fold change of that in the corresponding spheres. Data are presented as mean ± SD. $^{*}P < 0.05$, $^{**}P < 0.01$ compared with the control group.

monotherapy had no effect (Fig. 5g, h). These results suggested that the inhibition of cancer stemness, cell motility and lung metastasis by QAP14 is closely related to the activation of D1DR.

D1DR knockout accelerated metastasis and reversed the inhibitory efficacy of QAP14 in breast cancer

To further clarify the assumption that D1DR is the target of QAP14, 4T1-D1DR cells were generated and verified by Western blotting and immunofluorescence staining. As shown in Fig. 6a, b, D1DR was successfully knocked out in 4T1-D1DR cells. In contrast to the results in 4T1 cells, the relative colony count, wound width, and numbers of migrated and invaded 4T1-D1DR cells were virtually unchanged compared with those in the corresponding control groups (Fig. 6c–f). A minor impact of QAP14 was observed on the number and size of lung metastases in 4T1-D1DR allograft-bearing mice (Fig. 6g). Additionally, D1DR knockout in 4T1 cells increased migration and invasion in vitro (Fig. 6e, f) as well as lung metastasis in vivo (Fig. 6g). These findings further confirm that QAP14 exerts its anti-CSC, anti-motility and antimetastatic effects via D1DR activation.

QAP14 regulated the nuclear factor κB (NF-κB)/protein kinase B (Akt) pathway and the EMT process

To understand the antimetastatic mechanisms of QAP14, in addition to the increases in cAMP and cGMP levels by the activation of D1DR, the NF-κB/Akt pathway and the EMT process were investigated. As shown in Fig. 7a, QAP14 weakly changed the expression of the inhibitor of κB kinase subunit β (IKKβ) but dose-dependently reduced the level of phosphorylated IKKβ (p-IKKβ). QAP14 downregulated the expression of the inhibitor of κB subunit α (IκBα) at 12 μM but exerted a stronger inhibitory effect on the level of phosphorylated IκBα (p-IκBα) at both 6 and 12 μM. The level of NF-κB p65 (abbreviated p65) was unchanged after QAP14 treatment; however, the level of phosphorylated NF-κB p65 (abbreviated p-p65) in nuclei was significantly reduced. The regulatory effects of QAP14 on p65 and p-p65 were further confirmed by an immunofluorescence assay. As shown in Fig. 7b, there was no significant difference in the p65 level (represented by green fluorescence and also including p-p65) between the control and QAP14-treated groups. In contrast, the nuclear p-p65 level was significantly attenuated after QAP14 treatment. For Akt, treatment with 12 μM QAP14 for 48 h significantly decreased Akt phosphorylation, but little change in the level of total Akt was observed (Fig. 7c). These findings suggested that NF-κB/Akt signaling can be inhibited by QAP14 in 4T1 cells.

Since EMT is regarded as a key process required for metastasis, the effect of QAP14 on the EMT process in 4T1 cells was explored. QAP14 treatment considerably decreased the expression of MMP2, N-Cadherin, Slug, Snail and Vimentin, while E-Cadherin and ZO-1 were upregulated by QAP14, indicating that QAP14 inhibited the EMT process in 4T1 cells (Fig. 7d).

DISCUSSION

Metastasis is the major cause of death in breast cancer, and cancer stemness is a potential therapeutic target to reduce metastasis and improve patient survival. Several studies have found that D1DR activation may contribute to the elimination of CSCs and then inhibit cancer metastasis [11, 13–15]. However, straightforward evidence for the common effect of D1DR in cancer metastasis has not been presented, and the underlying mechanisms have just been preliminarily explored. In this study, we

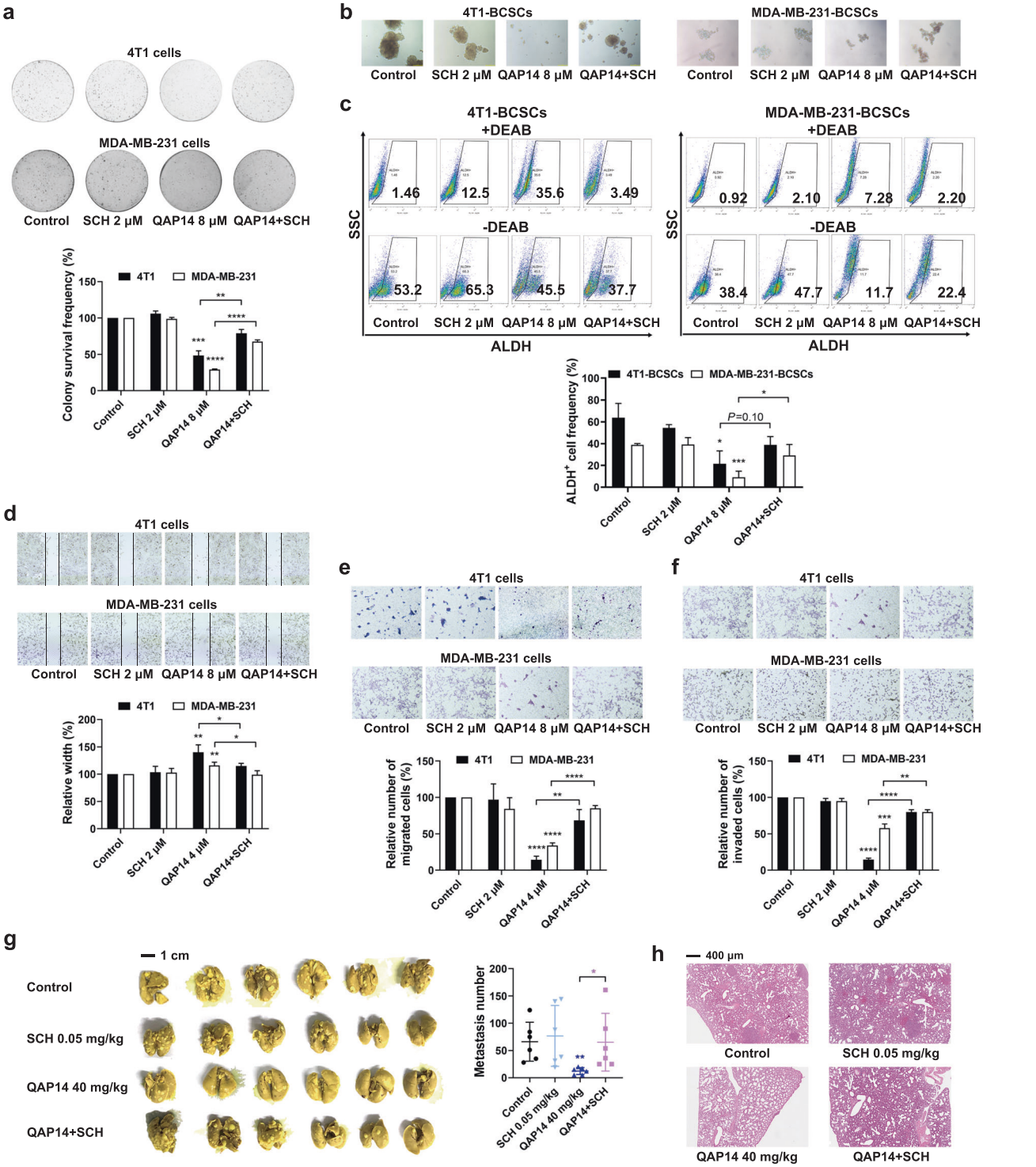

Fig. 5 D1DR antagonist SCH partially antagonized the regulatory effects of QAP14 on metastatic breast cancer. a 4T1 and MDA-MB-231 cells were treated with 8 μM QAP14 alone or in combination with 2 μM SCH for 48 h ($n = 3$ per group). Colonies at the end of experiment were shown. **b** Mammospheres derived from 4T1 and MDA-MB-231 cells were cultured with 8 μM QAP14 with or without 2 μM SCH for 48 h ($n = 3$ per group). Representative images were shown. **c** The ALDH-positive cell frequency of 4T1-BCSCs and MDA-MB-231-BCSCs were detected by flow cytometry after treatment with 8 μM QAP14 alone or in combination with 2 μM SCH for 48 h ($n = 3$). **d** Before being treated with 4 μM QAP14 and/or 2 μM SCH for 12 h, 4T1 and MDA-MB-231 cells were scratched with pipette tips, and the wound area of each group was pictured and measured at the end of experiments ($n = 3$). **e** 4T1 and MDA-MB-231 cells were exposed to 4 μM QAP14 alone or in combination with 2 μM SCH for 16 h and the images of migrated cells were recorded ($n = 3$). **f** Transwell invasion assay was used to detect cell invasion. Cells were cultured with 4 μM QAP14 with or without 2 μM SCH for 32 h (4T1 cells) and 24 h (MDA-MB-231 cells) ($n = 3$). **g** Photographs of the lungs taken out from the 4T1 tumor-bearing mice treated with QAP14 alone or in combination with SCH were shown and the number of metastatic nodules in each group was calculated ($n = 6$). The black scale bar indicates 1 cm. **h** Representative histopathological appearance of the lungs after H&E staining in each group was shown. The black scale bar indicates 400 μm. Data are presented as mean ± SD. $^{*}P < 0.05$, $^{**}P < 0.01$, $^{***}P < 0.001$, $^{****}P < 0.0001$ compared with the corresponding control group (if not indicated).

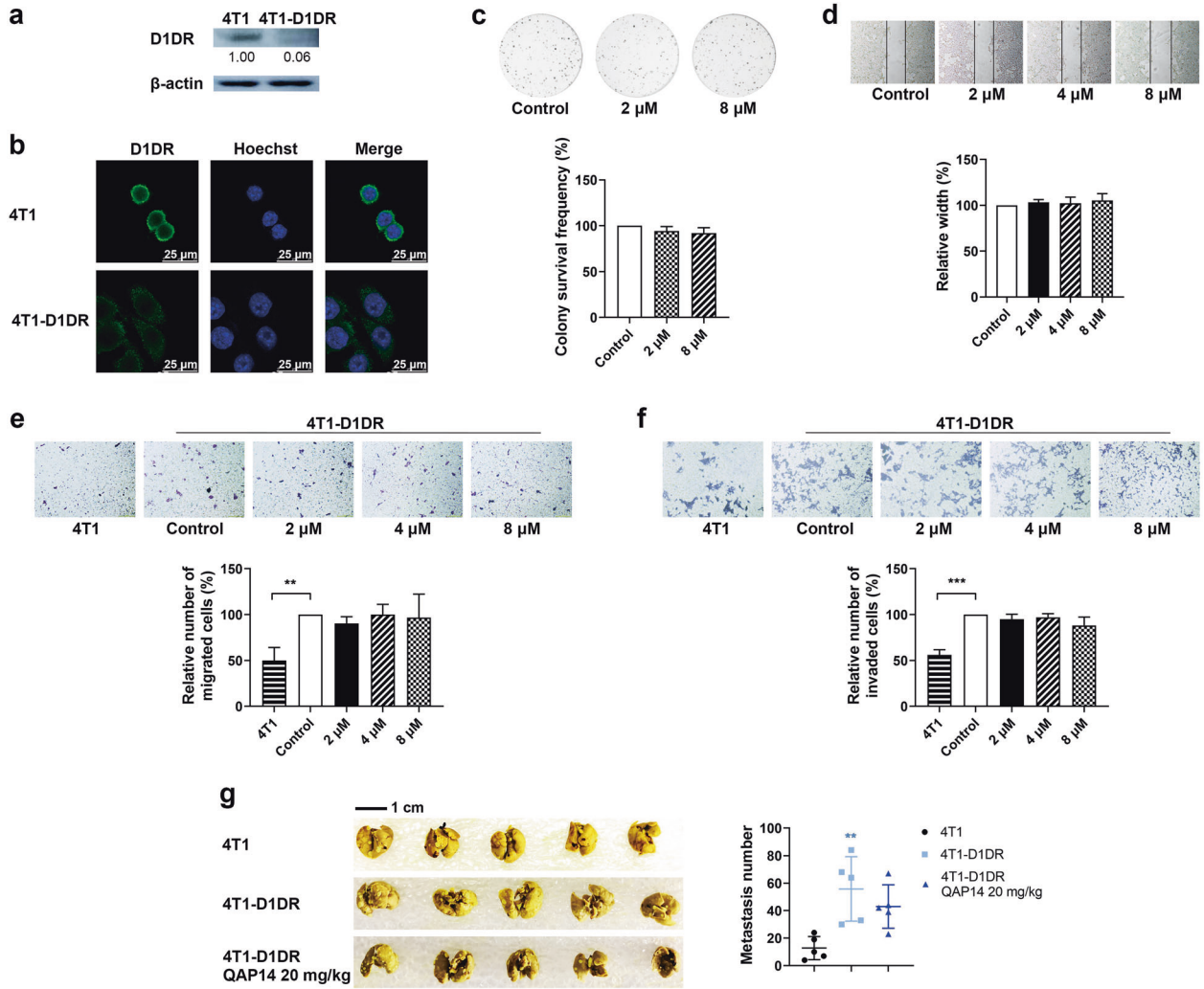

Fig. 6 D1DR knockout reversed the inhibitory efficacy of QAP14 on metastatic breast cancer. a The relative abundance of D1DR in 4T1 and 4T1-D1DR cells was detected by Western blotting ($n = 3$). **b** The D1DR expression in 4T1 and 4T1-D1DR cells was tested using immunofluorescence staining ($n = 3$). D1DR is indicated by green fluorescence and the nuclei are represented using blue fluorescence. The white scale bar indicates 25 μm. **c** 4T1-D1DR cells were treated with 0, 2, 8 μM QAP14 for 48 h. At the end of experiment, colonies of the control and the QAP14-treated groups were pictured and calculated ($n = 3$). **d** The effect of various concentrations of QAP14 on cell migration in 4T1-D1DR cells was assessed by wound healing assay. Both untreated 4T1 and 4T1-D1DR cells were added to the upper chambers and cultured for 16 h for transwell migration analysis (**e**) and 32 h for transwell invasion analysis (**f**), respectively ($n = 3$ per group). For 4T1-D1DR cells, the efficacy of different concentrations of QAP14 on cell migration and invasion was investigated at the same time. **g** The photographs of the lungs harvested from the mice administered with vehicle in 4T1 allograft model as well as the 4T1-D1DR-bearing mice who were treated with vehicle or QAP14 at the dose of 20 mg/kg. The average number of lung metastases in 4T1-bearing mice was set to 100% and the relative quantity was computed for the other groups ($n = 5$ per group). The black scale bar indicates 1 cm. Data are presented as mean ± SD. $^{**}P < 0.01$, $^{***}P < 0.001$ compared with the untreated 4T1 group.

directly confirmed the function of D1DR by establishing a D1DR-knockout 4T1 cell line and comprehensively investigated the mechanisms using a newly synthesized compound, QAP14. In addition, we found that QAP14 significantly suppressed cancer stemness and identified it as a potential therapeutic candidate agent for metastatic breast cancer.

Treatment with an antagonist of D1DR and knockout of D1DR were used together in this study to confirm the antimetastatic effect of D1DR activation. SCH is a D1DR antagonist that is frequently used to reverse the changes resulting from D1DR activation, thus verifying the involvement of D1DR [11, 13–15, 20–22]. However, the doses of SCH used for combination therapy may lead to incomplete occupancy, which means that SCH at nontoxic doses may fail to completely abolish the activation induced by D1DR agonists. Moreover, unknown targets or mechanisms of SCH may exist. In other words, treatment with SCH alone cannot sufficiently clarify the relationship among QAP14, D1DR and cancer metastasis. Therefore, gene knockout was performed in our study to confirm that D1DR is essential for the antimetastatic efficacy of QAP14.

To the best of our knowledge, only a few studies have identified the impact of DRs on tumor progression via knockout of DRs, and some of the studies corroborate our results. In pancreatic cancer, knockdown of D2DR was found to reduce proliferation, induce apoptosis, inhibit migration in vitro, as well as suppress tumor growth and metastasis [23]. In colorectal cancer, transient knockdown of D2DR was found to reduce the cell number, while stable downregulation of D2DR did not have significant effects on cell viability [24]. The above findings agree with our results that knocking out D1DR in 4T1 cells can promote their migration and invasion in vitro as well as their metastasis in vivo in this study, as the activation of D1- and D2-like receptors has inverse effects on the activity of adenylate cyclase (AC) and the production of cAMP

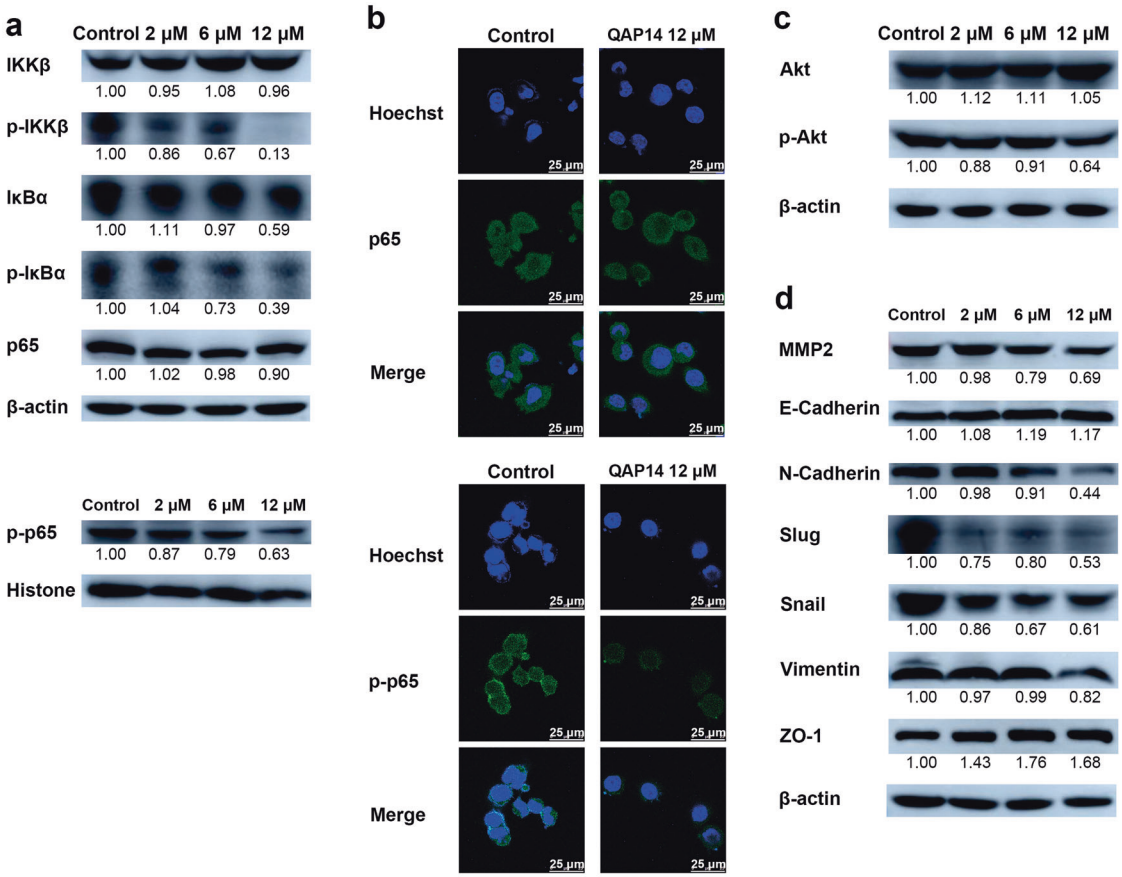

Fig. 7 QAP14 regulated NF-κB/Akt pathways and EMT process in 4T1 cells. **a** The effects of 2, 6, 12 μM QAP14 on NF-κB pathway were assessed by Western blotting ($n = 3$). **b** The expression and localization of p65 and p-p65 were detected by immunofluorescence imaging ($n = 3$). Green fluorescence represents p65 and p-p65, respectively, while blue fluorescence indicates the nuclei. The white scale bar indicates 25 μm. The regulatory efficacy of different concentrations of QAP14 on Akt pathway (**c**) and EMT process (**d**) was evaluated by Western blotting ($n = 3$). For Western blotting analysis, the value of the control group was set to "1", and the relative quantity was calculated for the treatment groups.

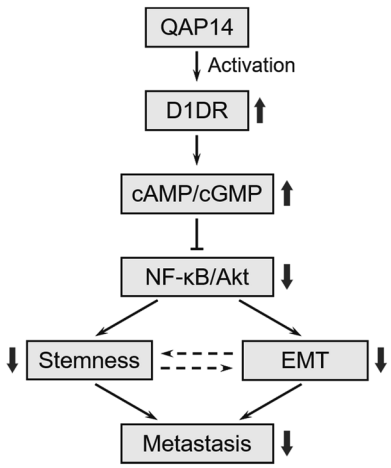

Fig. 8 The underlying mechanisms involved in the inhibitory effects of QAP14 via D1DR activation on breast cancer metastasis to the lung. The thin pointed and flat arrows represent the upregulated and downregulated effects, respectively. The dashed arrows indicate the crosslink between stemness and EMT. The thick upward or downward arrows indicate the effects of QAP14.

or cGMP [18, 19]. In contrast, in liver cancer, upregulation of D1DR expression was shown to significantly enhance cell proliferation, while downregulation of D1DR expression exerted the opposite effect [21]. The heterogeneity in both the roles and biological context of D1DR among distinct types of cells may account for the contradictory results [25]. Importantly, the in vitro and in vivo effects of QAP14 were completely reversed in the absence of D1DR, first revealing a direct relationship between D1DR activation and the antimetastatic efficacy of QAP14 in breast cancer. Moreover, the findings implied that D1DR is a potential target that is worthy of further investigation in metastatic cancers.

Metastasis-related intracellular signal transduction is mediated through a complex network. cAMP and cGMP are the second messengers produced when D1DR is stimulated [18, 19]. Accumulation of intracellular cAMP or cGMP can suppress the Akt pathway [26, 27], which cooperates with other signaling pathways, such as NF-κB, to mediate the EMT process and is involved in CSC enrichment and maintenance [28–32]. Crosstalk between EMT and CSCs, as well as their important roles in cancer metastasis, has been reported. Cancer cells undergoing EMT acquire CSC properties, while CSC-associated transcription factors such as Oct4 and Sox2 are in turn related to the regulation of EMT [33]. Therefore, regulation of the NF-κB/Akt pathway may contribute to suppression of metastasis via the inhibition of both stemness and the EMT process. The D1DR agonists FEN and l-SPD upregulated E-cadherin expression and downregulated MMP2 expression but had a minor influence on Vimentin expression in a 4T1 allograft model, implying their limited regulatory effects on the EMT process [13]. In comparison, QAP14 showed a marked influence on more markers implicated in these pathways. In 4T1-D1DR cells, the regulatory effects of QAP14 on most of the proteins closely related to these pathways, except for ZO-1 and E-Cadherin, were visibly

weakened compared with those in 4T1 cells (Supplementary Fig. S1). In general, these findings suggested that QAP14 increased cAMP and cGMP production via the activation of D1DR, and then suppressed NF-κB/Akt pathway activity and the EMT process as well as reduced the CSC population and breast cancer metastasis (Fig. 8). We did not exclude other signaling pathways that may be involved, such as the Notch, Wnt and sonic hedgehog pathways; therefore, further investigations will be conducted to confirm the mechanisms [34].

Compared with MDA-MB-231 cells, 4T1 cells formed rounder and denser spheroids, possibly partially due to different levels of epithelial phenotype markers, especially E-Cadherin [35]. The cellular level of ALDH is one of the most common hallmarks of CSCs; indeed, as few as 500 cells with high ALDH activity isolated from human breast tumors can induce tumor formation [36]. Thus, ALDH was chosen to identify the CSC subpopulation. A more significant increase in the CSC frequency and D1DR expression was observed in 4T1 mammospheres than in MDA-MB-231 mammospheres, which may account for the superior effects of QAP14 against 4T1-BCSCs compared with MDA-MB-231-BCSCs to a certain extent.

Despite the potency of QAP14 in decreasing cancer metastasis and prolonging the survival of 4T1 tumor-bearing mice, considering its limited effect on tumor growth, QAP14 may have higher clinical value when combined with other antitumor drugs. SUN, an antiangiogenic agent widely used in the clinical treatment of certain cancers, such as renal cell carcinoma, was found to increase the CSC frequency and hence enhance invasive and metastatic properties in human breast cancer xenografts [37]. Targeting D1DR could enhance the efficacy of SUN [11, 12, 14], although no experiments with a selective D1DR agonist, which could confirm the involvement of D1DR, have been conducted [25]. Therefore, we conducted an in vivo study to preliminarily investigate the effect of combination therapy with QAP14 and SUN. As expected, QAP14 enhanced the antitumor effect of SUN and suppressed cancer metastasis (Supplementary Fig. S2), thus suggesting a combination strategy for QAP14. In addition, in comparison to other D1DR agonists or analogs that we studied before [14, 15], the new compound QAP14 shows good PK characteristics and an acceptable safety profile, with a bioavailability of 50.29% and a terminal half-life of 8.67 h after oral administration, indicating that it has the greatest potential to be a drug candidate [38].

Murine 4T1 and human MDA-MB-231 cells are regarded as highly metastatic cells and are commonly used for research on cancer stemness and metastasis. In 4T1 cell line-derived models, the primary tumor grows at the anatomically orthotopic site after easy inoculation into the mammary gland; in addition, the cancer cells spontaneously metastasize from the primary tumor and spread to various organs, a process that is rather similar to that in human breast cancer [39]. Moreover, D1DR, which was speculated to be the target of QAP14, has been demonstrated to be expressed in both cell lines [13]. The effects of QAP14 on D1DR activation and lung metastasis in MDA-MB-231 cell line-derived models have not been assessed; hence, further research will be carried out to confirm this hypothesis. Since the cytotoxic IC_{50} values of QAP14 in 4T1 and MDA-MB-231 cells were 19.55 and 30.36 μM, respectively, a concentration of 12 μM, which was close to the IC_{20} values in both cell lines, was selected as the highest concentration of QAP14 for the in vitro study (Supplementary Fig. S3). For the in vivo study, the QAP14 dosing regimens were based on our previous research [15].

In summary, the role of D1DR activation in antimetastatic therapy was confirmed, and the new compound QAP14 exhibited substantial inhibitory effects on cell motility and cancer metastasis via D1DR activation, with an acceptable safety profile. The underlying mechanisms of QAP14 treatment involved blockade of the NF-κB/Akt pathway, reversion of the EMT process and inhibition of CSCs. This study provides an alternative strategy for targeting CSCs and suppressing metastasis via D1DR activation for the treatment of metastatic breast cancer.

ACKNOWLEDGEMENTS

This project was supported by the Beijing Municipal Natural Science Foundation (Grant No. 7192100) and National Natural Science Foundation of China (Grant No. 82073919).

AUTHOR CONTRIBUTIONS

Study conception and design: TYZ and LY; data acquisition: LY, GSC, XXY, YCG, and MYH; data analysis and interpretation: LY, YY, and JSX; manuscript drafting: LY, YY, and WZJ; critical revision: TYZ.

ADDITIONAL INFORMATION

Supplementary information The online version contains supplementary material available at https://doi.org/10.1038/s41401-021-00701-9.

Competing interests: The authors declare no competing interests.

REFERENCES

1. Chaffer CL, Weinberg RA. A perspective on cancer cell metastasis. Science. 2011;331:1559–64.
2. Gradishar WJ, Anderson BO, Abraham J, Aft R, Agnese D, Allison KH, et al. Breast Cancer, Version 3.2020, NCCN Clinical Practice Guidelines in Oncology. J Natl Compr Canc Netw. 2020;18:452–78.
3. Dittmer J. Breast cancer stem cells: features, key drivers and treatment options. Semin Cancer Biol. 2018;53:59–74.
4. Antoszczak M. A medicinal chemistry perspective on salinomycin as a potent anticancer and anti-CSCs agent. Eur J Med Chem. 2019;164:366–77.
5. Janzer A, German NJ, Gonzalez-Herrera KN, Asara JM, Haigis MC, Struhl K. Metformin and phenformin deplete tricarboxylic acid cycle and glycolytic intermediates during cell transformation and NTPs in cancer stem cells. Proc Natl Acad Sci USA. 2014;111:10574–9.
6. Shan NL, Wahler J, Lee HJ, Bak MJ, Gupta SD, Maehr H, et al. Vitamin D compounds inhibit cancer stem-like cells and induce differentiation in triple negative breast cancer. J Steroid Biochem Mol Biol. 2017;173:122–9.
7. Kakarala M, Brenner DE, Korkaya H, Cheng C, Tazi K, Ginestier C, et al. Targeting breast stem cells with the cancer preventive compounds curcumin and piperine. Breast Cancer Res Treat. 2010;122:777–85.
8. Sachlos E, Risueño RM, Laronde S, Shapovalova Z, Lee JH, Russell J, et al. Identification of drugs including a dopamine receptor antagonist that selectively target cancer stem cells. Cell. 2012;149:1284–97.
9. Li J, Yao QY, Xue JS, Wang LJ, Yuan Y, Tian XY, et al. Dopamine D2 receptor antagonist sulpiride enhances dexamethasone responses in the treatment of drug-resistant and metastatic breast cancer. Acta Pharmacol Sin. 2017;38:1282–96.
10. Yeh CT, Wu AT, Chang PM, Chen KY, Yang CN, Yang SC, et al. Trifluoperazine, an antipsychotic agent, inhibits cancer stem cell growth and overcomes drug resistance of lung cancer. Am J Respir Crit Care Med. 2012;186:1180–8.
11. Wang S, Mou Z, Ma Y, Li J, Li J, Ji X, et al. Dopamine enhances the response of sunitinib in the treatment of drug-resistant breast cancer: Involvement of eradicating cancer stem-like cells. Biochem Pharmacol. 2015;95:98–109.
12. Hao F, Wang S, Zhu X, Xue J, Li J, Wang L, et al. Pharmacokinetic-pharmacodynamic modeling of the anti-tumor effect of sunitinib combined with dopamine in the human non-small cell lung cancer xenograft. Pharmacol Res. 2017;34:408–18.
13. Yang L, Yao Y, Yong L, Feng Y, Su H, Yao Q, et al. Dopamine D(1) receptor agonists inhibit lung metastasis of breast cancer reducing cancer stemness. Eur J Pharmacol. 2019;859:172499.
14. Su H, Xue Z, Feng Y, Xie Y, Deng B, Yao Y, et al. N-arylpiperazine-containing compound (C2): An enhancer of sunitinib in the treatment of pancreatic cancer, involving D1DR activation. Toxicol Appl Pharmacol. 2019;384:114789.
15. Feng Y, Jiao P, Yan X, Xue Z, Yao Y, Yang L, et al. Compound C17 inhibits the lung metastasis of breast cancer. J Chin Pharm Sci. 2019;28:716–27.
16. Rajendran V, Jain MV. In vitro tumorigenic assay: colony forming assay for cancer stem cells. Methods Mol Biol. 2018;1692:89–95.
17. Cioce M, Gherardi S, Viglietto G, Strano S, Blandino G, Muti P, et al. Mammosphere-forming cells from breast cancer cell lines as a tool for the

identification of CSC-like- and early progenitor-targeting drugs. Cell Cycle. 2010;9:2878–87.
18. Borcherding DC, Tong W, Hugo ER, Barnard DF, Fox S, LaSance K, et al. Expression and therapeutic targeting of dopamine receptor-1 (D1R) in breast cancer. Oncogene. 2016;35:3103–13.
19. Beaulieu JM, Espinoza S, Gainetdinov RR. Dopamine receptors - IUPHAR Review 13. Br J Pharmacol. 2015;172:1–23.
20. Cherubini E, Di Napoli A, Noto A, Osman GA, Esposito MC, Mariotta S, et al. Genetic and functional analysis of polymorphisms in the human dopamine receptor and transporter genes in small cell lung cancer. J Cell Physiol. 2016;231:345–56.
21. Yan Y, Pan J, Chen Y, Xing W, Li Q, Wang D, et al. Increased dopamine and its receptor dopamine receptor D1 promote tumor growth in human hepatocellular carcinoma. Cancer Commun (Lond). 2020;40:694–710.
22. Bourne JA. SCH 23390: the first selective dopamine D1-like receptor antagonist. CNS Drug Rev. 2001;7:399–414.
23. Jandaghi P, Najafabadi HS, Bauer AS, Papadakis AI, Fassan M, Hall A, et al. Expression of DRD2 is increased in human pancreatic ductal adenocarcinoma and inhibitors slow tumor growth in mice. Gastroenterology. 2016;151:1218–31.
24. Kline CLB, Ralff MD, Lulla AR, Wagner JM, Abbosh PH, Dicker DT, et al. Role of dopamine receptors in the anticancer activity of ONC201. Neoplasia. 2018;20:80–91.
25. Sobczuk P, Łomiak M, Cudnoch-Jędrzejewska A. Dopamine D1 receptor in cancer. Cancers. 2020;12:3232.
26. Jiang K, Yao G, Hu L, Yan Y, Liu J, Shi J, et al. MOB2 suppresses GBM cell migration and invasion via regulation of FAK/Akt and cAMP/PKA signaling. Cell Death Dis. 2020;11:230.
27. Kim S, Jee K, Kim D, Koh H, Chung J. Cyclic AMP inhibits Akt activity by blocking the membrane localization of PDK1. J Biol Chem. 2001;276:12864–70.
28. Maier HJ, Schmidt-Strassburger U, Huber MA, Wiedemann EM, Beug H, Wirth T. NF-kappaB promotes epithelial-mesenchymal transition, migration and invasion of pancreatic carcinoma cells. Cancer Lett. 2010;295:214–28.
29. Liu M, Sakamaki T, Casimiro MC, Willmarth NE, Quong AA, Ju X, et al. The canonical NF-kappaB pathway governs mammary tumorigenesis in transgenic mice and tumor stem cell expansion. Cancer Res. 2010;70:10464–73.
30. Huber MA, Azoitei N, Baumann B, Grünert S, Sommer A, Pehamberger H, et al. NF-kappaB is essential for epithelial-mesenchymal transition and metastasis in a model of breast cancer progression. J Clin Invest. 2004;114:569–81.
31. Butti R, Gunasekaran VP, Kumar TVS, Banerjee P, Kundu GC. Breast cancer stem cells: Biology and therapeutic implications. Int J Biochem Cell Biol. 2019;107:38–52.
32. Bakin AV, Tomlinson AK, Bhowmick NA, Moses HL, Arteaga CL. Phosphatidylinositol 3-kinase function is required for transforming growth factor beta-mediated epithelial to mesenchymal transition and cell migration. J Biol Chem. 2000;275:36803–10.
33. Babaei G, Aziz SG, Jaghi NZZ. EMT, cancer stem cells and autophagy; the three main axes of metastasis. Biomed Pharmacother. 2020;133:110909.
34. Taurin S, Alkhalifa H. Breast cancers, mammary stem cells, and cancer stem cells, characteristics, and hypotheses. Neoplasia. 2020;22:663–78.
35. Manuel Iglesias J, Beloqui I, Garcia-Garcia F, Leis O, Vazquez-Martin A, Eguiara A, et al. Mammosphere formation in breast carcinoma cell lines depends upon expression of E-cadherin. PLoS One. 2013;8:e77281.
36. Ginestier C, Hur MH, Charafe-Jauffret E, Monville F, Dutcher J, Brown M, et al. ALDH1 is a marker of normal and malignant human mammary stem cells and a predictor of poor clinical outcome. Cell Stem Cell. 2007;1:555–67.
37. Conley SJ, Gheordunescu E, Kakarala P, Newman B, Korkaya H, Heath AN, et al. Antiangiogenic agents increase breast cancer stem cells via the generation of tumor hypoxia. Proc Natl Acad Sci USA. 2012;109:2784–9.
38. Guo Y, Yao Q, Kong D, Xue J, Yong L, Li J, et al. Development and validation of a highly sensitive HPLC-MS/MS method for the QAP14, a novel potential anti-cancer agent, in rat plasma and its application to a pharmacokinetic study. J Pharm Biomed Anal. 2020;189:113487.
39. Pulaski BA, Ostrand-Rosenberg S. Mouse 4T1 breast tumor model. Curr Protoc Immunol. 2001; Chapter 20: Unit 20.2.